Analysis of Partial Volume Correction on Quantification and Regional Heterogeneity in Cardiac PET

A. Turco, PhD[a], J. Nuyts, PhD[a], J. Duchenne, MSc[b], O. Gheysens, MD, PhD[a,c], J.U. Voigt, MD, PhD[b,d], P. Claus, PhD[b], K. Vunckx, PhD[a]

[a] *KU Leuven - University of Leuven, Department of Imaging and Pathology, Nuclear Medicine and Molecular imaging, Medical Imaging Research Center (MIRC), B-3000 Leuven, Belgium.*
[b] *KU Leuven - University of Leuven, Department of Cardiovascular Sciences, Cardiology, Medical Imaging Research Center (MIRC), B-3000 Leuven, Belgium.*
[c] *University Hospitals Leuven, Department of Nuclear Medicine, B-3000 Leuven, Belgium.*
[d] *University Hospitals Leuven, Department of Cardiovascular Diseases, B-3000 Leuven, Belgium.*

Abstract

Background. The partial volume correction (PVC) of cardiac PET datasets using anatomical side information during reconstruction is appealing but not straightforward. Other techniques, which do not make use of additional anatomical information, could be equally effective in improving the reconstructed myocardial activity.

Methods. Resolution modelling in combination with different noise suppressing priors was evaluated as a means to perform PVC. Anatomical priors based on a high-resolution CT are compared to non-anatomical, edge-preserving priors (relative difference and total variation prior). The study is conducted on *ex vivo* datasets from ovine hearts. A simulation study additionally clarifies the relationship between prior effectiveness and myocardial wall thickness.

Results. Simple resolution modelling during data reconstruction resulted in over- and under- estimation of activity, which hampers the absolute left-ventricular quantification when compared to the ground truth. Both the edge-preserving and the anatomy-based PVC techniques improve the absolute quantification, with comparable results (Student t-test, $p = 0.17$). The

relative tracer distribution was preserved with any reconstruction technique (repeated ANOVA, p = 0.98).

Conclusions. The use of edge-preserving priors emerged as optimal choice for quantification of tracer uptake in the left-ventricular wall of the available datasets. Anatomical priors visually outperformed edge-preserving priors when the thinnest structures were of interest.

Keywords: cardiac PET, system resolution, partial volume correction, quantification

---

List of abbreviations

PET ..... Positron Emission Tomography
(HR)CT... (High Resolution) Computed Tomography
PVE ..... Partial Volume Effect
PVC ..... Partial Volume Correction
OSEM .... Ordered Subsets Expectation Maximisation (reconstruction algorithm)
RR ..... Resolution Recovery
MAP ..... Maximum-a-Posteriori (reconstruction algorithm)
TV ..... Total Variation (prior)
RD ..... Relative Differences (prior)

1. Introduction

Positron emission tomography (PET) is a sensitive and quantitatively precise preclinical and clinical tool for cardiovascular applications. ^{18}F-FDG PET is nowadays the most sensitive method to identify myocardial viability [1, 2]. Cardiac PET imaging leads to a panel of clinically relevant parameters that can be interpreted visually (viability, tracer uptake in plaques or sarcoid lesions, regional differences in tracer uptake) but some of these require a quantitative analysis (absolute blood flow, function). Quantification improves reproducibility, reduces inter-observer variability and might enhance the diagnostic accuracy [3].

Despite the wide range of applications for cardiac PET, the resulting images inherently suffer from severe blurring, due to both the finite resolution

of the imaging system (partial volume effect, PVE) and cardiac and respiratory motion during the entire PET examination [4], both of which hamper accurate quantification. The use of partial volume correction (PVC) techniques based on high resolution anatomical information to correct for this PVE has been successfully applied for PET brain imaging and to restore cardiac lesion uptake in a simulation study. In both cases, this resulted in improved quantitative information [5, 6, 7].

The main objective of this study is to evaluate the influence of two types of advanced reconstruction algorithms (anatomy-based and edge-preserving priors) on regional quantification of the left myocardial ventricle (LV) in comparison to the currently used clinical algorithms (with or without resolution modelling). All algorithms were applied on *ex vivo* datasets excised from sheep with asymmetric cardiac remodelling. The use of *ex vivo* (static) datasets allowed to rule out quantification errors caused by cardiac or respiratory motion, and could therefore be considered as an ideal version of a single frame from a doubly gated *in vivo* study.

The animal model used in this work was an ovine model of dilated cardiomyopathy with asymmetric left ventricular remodelling due to a left-bundle branch block-like conduction delay. Some of the typical features of this pathology are a dilation of the LV chamber over time, together with a thinning of the septal wall and a thickening of the lateral wall of the LV during the progression of the disease. Such variations in the wall thicknesses were hypothesised to generate problems with relative tracer uptake quantification, due to the partial volume effects which are expected to mostly affect the thinned walls. The application of PVC techniques in hearts which underwent such kind of remodelling should best demonstrate the recovery of activity in the thinnest walls, provided that the final wall thinning is enough to cause severe PVEs.

2. Methods

2.1. Animal model and experimental design

We used an ovine model of rapid pacing-induced dilated cardiomyopathy with left-bundle branch block-like morphology leading to asymmetric remodelling of the septal and lateral wall. All experiments and procedures were approved by the local ethical committee.

Each of the thirteen available sheep was sacrificed and their heart was excised. The excised, *ex vivo* hearts were filled with a non-attenuating, hard-

ening poly-urethane foam in order to ensure a stable shape of the heart in time. Each heart was filled once throughout the experiment, hence the heart shape was always the same throughout the *ex vivo* scans of the same animal. A pilot *ex vivo* experiment had been previously carried out to confirm that the foam would not keep on expanding throughout the duration of the imaging process. The following *ex vivo* scans were performed:

- a 15-minute acquisition on a small-animal PET scanner (Siemens Focus220 microPET), which served as gold standard because of the high spatial resolution of this PET system (1.5 mm), resulting in images that are almost free from resolution-related blurring. A transmission scan with a rotating ^{57}Co point source was also obtained for scatter correction.

- a 20-minute PET scan on the clinical PET/CT scanner (Siemens Biograph 16, Hirez). These datasets were reconstructed with different algorithms and compared to the ground truth images provided by the microPET.

- a high-dose, high-resolution CT (HRCT) on the clinical PET/CT scanner. It was used for accurate attenuation correction and for PVC of both the clinical and the microPET datasets. In the *ex vivo* hearts the blood is removed from the ventricular cavities and the polyurethane foam is injected in their place. This allows a clear distinction of the myocardium, thus ensuring an efficient PVC. No contrast-enhanced CT is therefore needed in this case.

2.2. Simulation study

A simulation study was designed to clarify whether there is a relationship between the apparent thickness of the reconstructed structures and the different reconstruction algorithms.

For this purpose, several cylindrical phantoms resembling the shape of the left ventricle were designed, all with a height of 65 mm and an outer diameter of 30 mm. The cylindrical walls of each phantom had a uniform thickness, which was different for each phantom and ranged between 1 and 12 mm (representative of the thicknesses that can be encountered in a cardiac setting). Figure 1 shows one of the designed phantoms.

The walls of the phantom were filled with a known and fixed activity concentration of 4 kBq/cc. A second identical phantom was then created

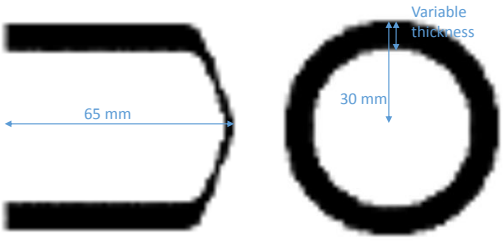

Figure 1: Transaxial (left) and axial (right) view of one of the phantoms simulated to demonstrate the effect of the reconstruction algorithms against different phantom thicknesses. The arrow with *Variable thickness* indicates the part of the phantom that was modified in the subsequent simulations to study the effect of different wall thicknesses (in this example, the wall thickness is 8 mm).

to simulate a uniform attenuation map and filled with a known and fixed attenuation value of 0.0999428 (attenuation $\times$ cm^{-1}), which corresponds to the mean attenuation value found for muscle at 511 keV [8]. A third copy of the phantom was used to simulate the anatomical prior information, perfectly aligned to the emission dataset.

A simulated acquisition of each of these numeric phantoms was performed, modelling the physical phenomena of limited spatial resolution, attenuation and detector normalization. Scatter and randoms were not modelled to exclude their influence from the analysis. A noise-free sinogram was obtained for each phantom. The resulting total sinogram counts are between 0.5 and 2.5 million counts, depending on the phantom thickness. This is in the same order of magnitude as the total sinogram counts of the available heart datasets with the lowest uptake and a 20 min data acquisition. One noisy sinogram was generated for each thickness-phantom by adding Poisson noise to the noise-free sinogram.

2.3. Image reconstruction

Hirez PET/CT datasets

Both simulated and real measured datasets were reconstructed using the same iterative reconstruction scheme ([3,2,2] iterations $\times$ [42,24,1] subsets). A realistic, in-house developed model of the Hirez PET system was used both for the simulated acquisition of the numeric phantoms and for the reconstruction of all the Hirez PET datasets. When requested, the spatial resolution of the scanner was modelled as a Gaussian function whose full-width at half-maximum corresponds to the spatial resolution of the scanner (4.3 mm and

4.5 mm in the transaxial and axial direction, respectively). The voxel size of the reconstructed PET images was set to $1.35 \times 1.35 \times 1.35$ mm^3 for all datasets.

An overview of the different algorithms used to reconstruct each of the available sinograms is listed below:

1. iterative reconstruction (ordered subsets expectation maximisation, **OSEM**) without resolution recovery (RR)
2. OSEM with RR (**OSEM + RR** in the rest of this work), which takes into account the resolution of the scanner during the PET reconstruction.
3. iterative reconstruction with prior information (maximum-a-posteriori, MAP) with RR, with CT-based side anatomical information. The anatomical information was incorporated in the reconstruction process by means of the asymmetrical **Bowsher** prior [9, 10]. The Bowsher prior is parametrised by two values, namely the weight (w) and the number of neighbours (n), which define the strength of the prior and the size of its smoothing mask respectively.
4. MAP with RR in combination with a non-anatomy based prior (known as *relative differences* (**RD**) prior [11]), parametrised by a weight (w) and an edge-preserving parameter (γ).
5. MAP with RR, in combination with a non-anatomy based prior (known as *isotropic total variation prior* (**TV**) [12]), parametrised by a weight (w).

A range of prior parameter values was chosen based on a simulation study, where reconstructions with a similar count level were compared to a ground truth dataset in terms of bias and noise. A visual inspection of the datasets confirmed that the chosen range was an appropriate compromise between noise reduction and excessive smoothing of the structures.

microPET datasets

The microPET list-mode datasets of the *ex vivo* hearts were reconstructed using a MAP reconstruction algorithm (5 iterations $\times$ 28 subsets) with resolution recovery [13] and asymmetrical Bowsher prior (w = 50, n = 9). We chose to apply a prior because resolution recovery alone is known to reduce the apparent thickness of the structures and to possibly hamper quantification [14]. Moreover, Bowsher reconstructions have been shown to improve the recovery of activity concentrations in previous studies, e.g. in [6]. In order to

corroborate such findings and choose which microPET reconstruction to use as ground truth, we performed a preliminary simulation study. The Bowsher reconstruction with the aforementioned parameters was found to minimise the bias and the noise when compared to a simulated ground truth. It was therefore chosen as the reconstruction method for the microPET datasets in this study.

Attenuation correction of the microPET was based on the HRCT and performed, together with scatter and sensitivity correction, during reconstruction. The data were also precorrected for randoms and deadtime. The microPET images were reconstructed with a voxel size of $0.4745\times$ $0.4745\times$ 0.796 mm^3. For comparison to the Hirez datasets, they were rigidly aligned and resampled to match the Hirez.

2.4. Image post-processing

A polar map (or bull's eye) representation of the simulated and *ex vivo* reconstructions was chosen to illustrate the regional and absolute differences within the myocardium. To create the bull's eye plots, the software must compute a single value for each longitudinal and angular position within the LV. This value must represent the activity over the LV wall thickness at each of those positions. To do so, the LV wall portion enclosed by the endocardial and the epicardial contours is considered for each angular and longitudinal position. The definition of the endocardial and epicardial contours is done automatically using a model-based approach, as described in [15]. The maximum activity value or the mean activity value along each of those portions is computed (see [7] for further details on the process). This value is then used to represent the activity value over the myocardial thickness. Both types of polar maps were created in this work, by taking the maximum or the mean count over the LV thickness (*max-count* and *mean-count* polar maps in the rest of this work, respectively).

2.5. Image analysis

Measured ex vivo datasets

The **absolute** values of the *ex vivo* reconstructions were compared. The mean difference between the microPET polar map and the *ex vivo* Hirez polar maps, relative to the mean activity of the microPET polar map, was computed and plotted, for each animal. The values extracted from the mean-count polar maps were compared to the values extracted from the max-count polar maps.

For every polar map, the S/L ratio was additionally calculated by dividing the mean activity in the free septal wall (segments 8, 9 in a conventional 17-segment polar map [16]) by the mean activity in the free lateral wall (segments 11, 12). This analysis aimed to quantify whether the prior-based reconstructions improve or preserve the **regional variations** of activity within the heart, when compared to the S/L ratio computed on the polar map of the corresponding ground truth reconstructions.

Although the analysis of the septal vs lateral walls is commonly performed to describe regional inhomogeneity in the heart function and metabolism [17], a more general overview of the inhomogeneities was also provided. To this end, each of the available *ex vivo* max-count polar maps was considered, and divided by its maximum to obtain a *normalized* polar map (unit-less, ranging between 0 and 1). For each sheep, all the normalized polar maps from the Hirez scanner, obtained with the different reconstruction techniques, were compared to the normalized polar map of the ground truth. The resulting percentage bias was computed, per segment. The mean of the segmental biases was computed over all the sheep, together with the segmental standard deviation of the bias over all sheep. Two corresponding polar maps were generated for each reconstruction algorithm, whose segmental values represent the mean bias and the mean standard deviation of the normalized polar maps of the Hirez against the ground truth.

Simulated datasets

The mean activity in the middle ring of each max-count polar map of the simulated phantoms was plotted for the different phantom thicknesses in comparison to the activity expected in that region (4 kBq/cc).

Additionally, profiles through the wall were taken in the cylindrical part of the heart phantom (Figure 1). An average of the 20 central subsequent axial profiles was considered, to minimise the contribution of noise to the profiles. These mean profiles were plotted for all different reconstruction algorithms.

2.6. Statistical methods

A repeated ANOVA between the different reconstructions of the measured datasets was performed, to establish whether a statistical difference in the mean absolute activity differences could be found, and the resulting p and F values were reported (significance level: 0.05). An additional Student t-test with posthoc Bonferroni correction helped to point out the algorithms

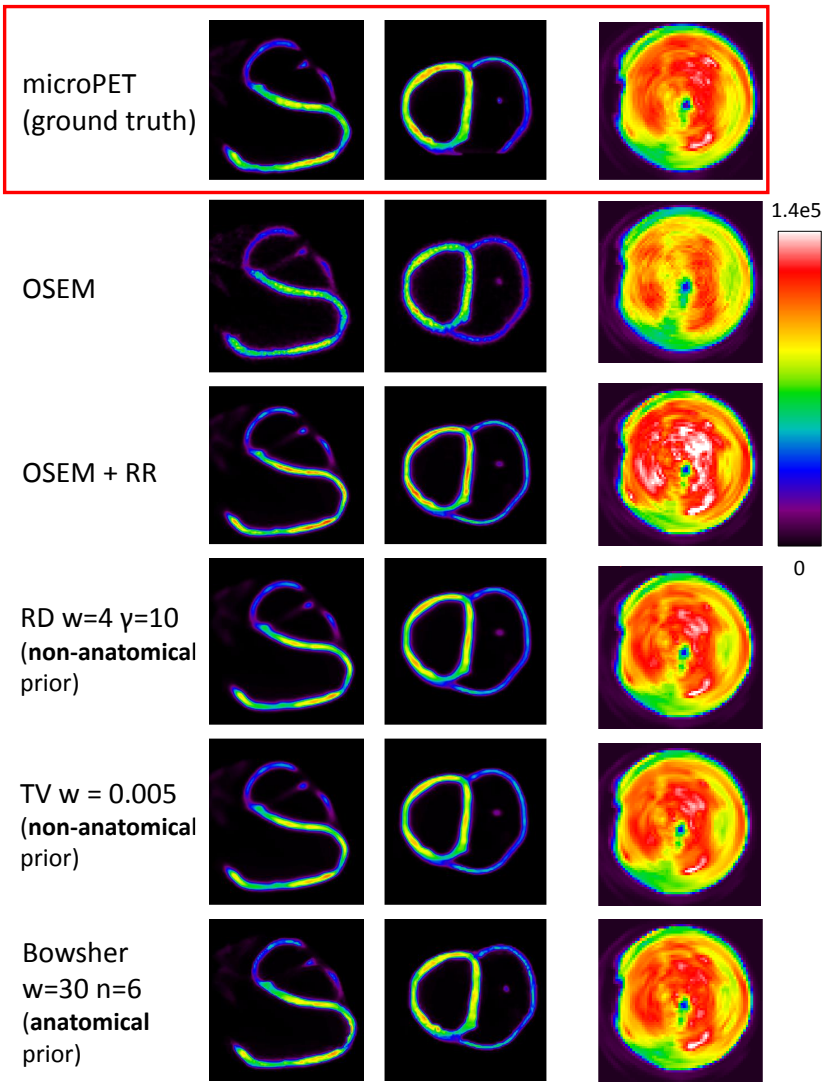

Figure 2: Representative images of an *ex vivo* sheep heart (sheep4238) reconstructed with different algorithms. On the right, the corresponding max-count polar maps for the same sheep are shown. The red box highlights the ground truth dataset (microPET). Color scale in Bq/cc. OSEM: ordered-subsets expectetion-maximization (iterative reconstruction) algorithm, RR: resolution recovery, RD: relative differences prior, TV: total variation prior.

which significantly differed from the state-of-the-art reconstruction technique (OSEM + RR). A repeated ANOVA test between the mean S/L ratios computed from the various reconstructions was also performed, and the resulting p and F values were reported (significance level: 0.05).

3. Results

Measured ex vivo datasets

A representative dataset with a selection of the performed reconstructions is shown in Figure 2. The use of well tuned edge-preserving priors (RD, TV) seems to work as well as a (well tuned) Bowsher prior, even though the Bowsher reconstructions show moderately sharper edges. In all cases, the visual assessment of the different reconstructions did not reveal dramatic changes in the relative activity distribution. The polar maps obtained for all the ex vivo datasets were also compared visually (right column of Figure 2) and confirmed the previous observations.

The accurate **absolute recovery** of the activity concentrations within the LV was then considered (Figure 3), which confirms an overall underestimation of the mean LV activity when no resolution recovery is modelled and a significant mean overestimation of the LV activity for the reconstructions with resolution recovery alone (repeated ANOVA: F-value=150, p-value < 0.001 (significant)). The T-test between TV and the latter (OSEM+RR) gives a p-value < 0.001 (significant), whereas the same test between TV and Bowsher w=30,n=9 has a p-value of 0.17 (not significant). This ranking holds true when the mean-count polar maps are used (bottom pane of Figure 3), but the differences between the different algorithms are more subtle. However, we can clearly appreciate the stabilizing role of the regularization included during the reconstruction process.

The **S/L ratios** were further calculated for the polar maps of each of the clinical reconstructions. They were compared to the ground truth S/L ratio extracted from the corresponding microPET reconstruction. Within each animal, the S/L ratios do not significantly change with different reconstruction algorithms, further supporting our visual evaluation of the polar maps. The ANOVA test showed no significant differences in the mean S/L ratios recovered from the different reconstruction algorithms ($F = 0.25$, $p = 0.98$).

The polar maps describing the mean bias and the mean standard deviation of the bias, over all sheep, are reported in Figure 4 for 4 selected

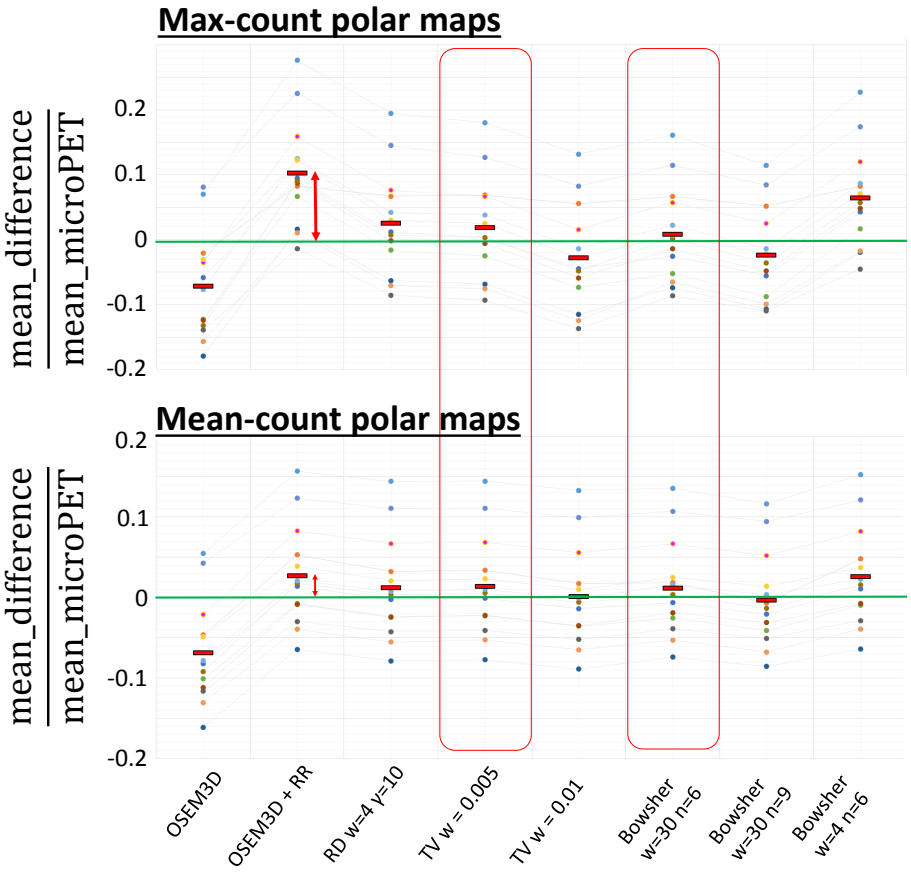

Figure 3: Mean difference between the polar maps of the ground truth (microPET) and the polar maps of the *ex vivo* Hirez images, reconstructed with the various algorithms, relative to the mean activity of the polar map of the corresponding microPET. Connected dots of the same color represent individual animals. The red solid bar is the mean value over all animals for each of the considered algorithms. The use of a different way to obtain the polar maps (max-count (top) or mean-count (bottom) polar maps) changes the amount of error that is computed, especially for OSEM+RR (red arrows). The use of edge-preserving or anatomical priors leads to a more accurate and more stable absolute quantification of the activity in the LV, regardless of the type of polar map that is used. The red boxes highlight this behaviour for two representative cases.

algorithms: Bowsher (weight=30, n=9), TV (weight=0.005) and for the iterative reconstruction with and without resolution recovery. Most of the individual biases are within the ±0.1 threshold, thus indicating very small differences (up to 10%) in the reconstructed LV homogeneity.

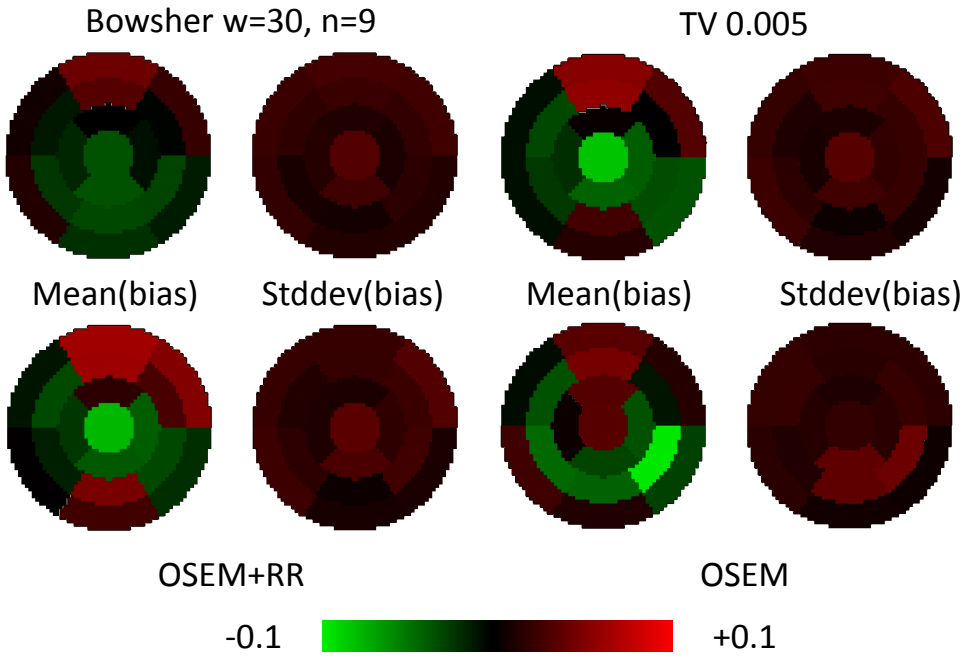

Figure 4: Mean bias (left side of each quadrant) and mean standard deviation of the bias (right side in each quadrant) over all animals, extracted from the normalized max-count polar maps of the reconstructions using a selection of the different algorithms. OSEM: iterative reconstruction, with or withour resolution recovery (RR); TV: non-anatomical prior, Bowsher: anatomical prior. The bias is a fraction of the maximum of the normalized polar maps, i.e. a fraction of 1.

Simulated datasets

The analysis of the mean reconstructed activity at different phantom thicknesses is in Figure 5. As hypothesized, the thinnest phantoms benefit more from the additional use of anatomical information (black line), while the non-anatomical priors – or the anatomical priors where the number of neighbours over which the smoothing is performed is too large – blur over the edges and therefore struggle to fully restore the activity within the walls of the thinnest phantoms. The iterative reconstruction with resolution recovery

alone displays the typical overestimation of activity at a thickness of 6-8 mm (roughly double the spatial resolution of the system), which becomes less apparent with increasing wall thickness of the cardiac phantom ($\geq$ 10 mm).

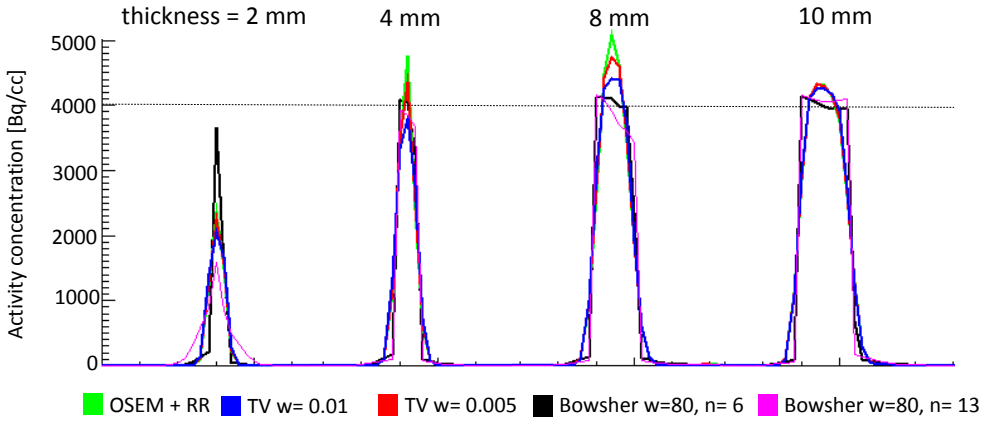

Figure 5: Profiles over one wall of the heart phantom (simulated homogeneous activity of 4 kBq/cc), for a selection of phantom thicknesses. To emphasize the effect of the parameter choice in the Bowsher reconstructions, especially at small thicknesses, a high weight and two very different numbers of neighbours (n) are shown.

The analysis of the mean recovered value in the max-count bull's eye plots of the heart phantom at different thicknesses (Figure 6) confirms the findings of the profile analysis and of the analysis of the *ex vivo* measured datasets.

The visual inspection of the thinnest structures of the sheep datasets (e.g. right ventricle) confirms the improved reconstruction of such areas when an adequately chosen anatomical prior is used. Figure 7 shows a comparison between the short-axis slices of two Bowsher and two TV reconstructions.

4. Discussion

The use of anatomical side information for the improved quantification of cardiac PET datasets stemmed from previous, successful experiences in brain PET imaging, where similar techniques have been applied during the reconstruction of PET datasets [6]. The results obtained in the current study are in line with previous findings and add interesting insights into the discriminating factors for choosing an anatomy-based prior.

The modelling of the resolution during reconstruction is essential for dealing with the PVE. However, our findings confirm that the resolution recovery

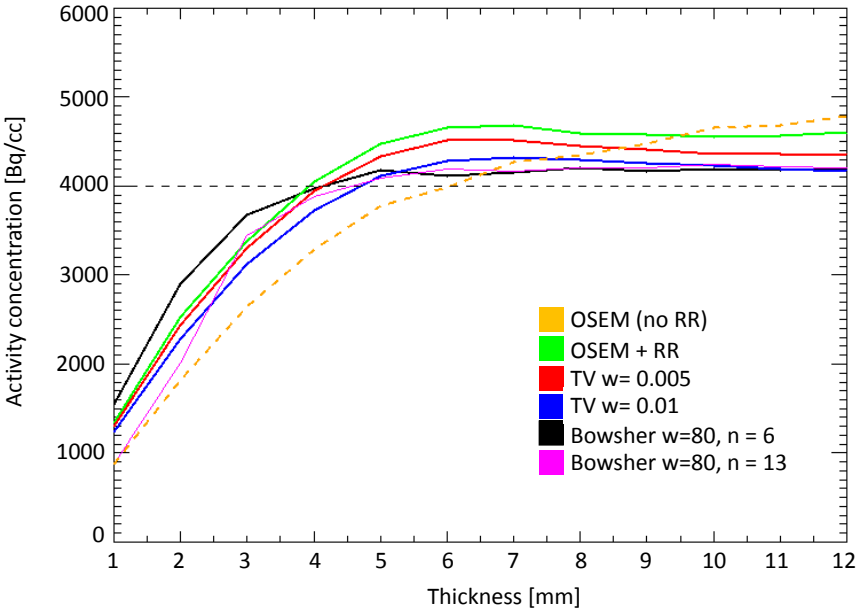

Figure 6: Mean value in the max-count polar maps of the heart phantoms, at increasing phantom thicknesses. The Bowsher algorithm, with a well chosen neighborhood, is the one that best improves the recovery of the mean activity concentration starting from a thickness of 2 mm.

is an ill-posed problem [18] and, alone, is not sufficient for accurate image quantification. Some kind of regularization is additionally needed to produce more quantitatively accurate results. In this study, the use of priors proves to improve the absolute quantification of the left ventricles, when compared to the state-of-the-art iterative reconstruction algorithms (with or without resolution recovery). This paper highlights the role of both anatomical (Bowsher) and non-anatomical edge-preserving priors (RD, TV) applied during the reconstruction of the datasets in stabilizing the resulting images. Even when the weights or the number of neighbours chosen are not fully optimized for the structures of interest (e.g. too many neighbours, or too bland prior weight), the error calculated in the enhanced reconstructions is milder than the one obtained in the reconstructions where no priors are used.

For regional analysis and relative quantification of the activity distribution within the left ventricle, on the other hand, the use of either reconstruction algorithm (with or without prior information) was sufficient and provided similar information. The S/L ratios are equally well resolved when

Figure 7: Comparison between non-anatomical (TV) and CT-based Bowsher reconstructions, for three different sheep datasets (from left to right column: sheep4238, sheep1869 and sheep1132). For both algorithms, the same short-axis slice and the same maximum is shown (they differ for the different animals, to maximize visibility).

compared to the ground truth ratio, no matter the reconstruction algorithm that is chosen for reconstructing the datasets obtained on the clinical scanner.

It is worth mentioning that the Bowsher priors presented in the study on the wall thickness for demonstrative purposes use a considerably high weight to achieve such results. In a more realistic scenario where these techniques would be applied, i.e. a motion-corrected acquisition with the use of anatomical information obtained from a dedicated scanner, the use of a high weight would be risky and could cause artefacts if the alignment between the PET and the anatomical dataset is not accurate. To present, the prior parameters need to be tuned in a case-by-case fashion to obtain optimal results, which can be a limiting factor for a realistic clinical workflow. A way to automatically select the best prior parameters was out of the scope of this work and should be subject of further investigation. Additionally, it is necessary to underline the importance of a correct image alignment and motion correction, before proceeding to anatomy-based PET reconstruction. With these regards, truly simultaneous PET/MR systems might represent a great improvement in the direction of accurate alignment, provided that the technical advances in MRI imaging will reduce the geometrical distortions and artefacts that nowadays still affect the gated MR measurements [19].

A limitation of this study is the sole use of *ex vivo*, static cardiac datasets for the assessment of the usefulness of partial volume correction techniques. In patients, the motion of the heart due to the beating and the breathing during the scan can create additional blurring of the PET datasets and needs to be taken into account and fully corrected if accurate quantification is aimed at. We expect a worsening of the quantification performances of any of the presented algorithms in the case where the correction of the motion is inaccurate or missing. The use of *in vivo* datasets, which we acquired within the same study as the *ex vivo* datasets, should help to shed further light into the applicability of the presented techniques to images of the beating heart. The analysis of the *in vivo* datasets is ongoing. Particularly, given that no partial volume correction technique should be applied to datasets that are not corrected for motion, we are investigating on the applicability of partial volume correction techniques in combination with dual-gating techniques. The results of the *in vivo* study will be made available upon completion. A particularly important conclusion from the present *ex vivo* study, where no motion is present and alignment with anatomical data is perfect, is that non-anatomical priors and anatomical, CT-based priors perform equally well for the quantification of LV activity. As the current *ex vivo* experiment can be considered as an ideal dual-gated *in vivo* experiment – where the scatter, attenuation and motion correction have been perfectly accounted for–, we believe that the application of non-anatomy based priors is a good starting point for truly dual-gated *in vivo* studies where the LV walls are of interest. This is advantageous as it simplifies the overall acquisition and reconstruction process.

Finally, although the application of non-anatomical priors yielded acceptable quantification results on the available animal cohort (i.e. hearts without lesions and with sufficiently thick LV walls), the application of anatomical information for cardiac PET imaging is not to be fully excluded, particularly when non-transmural lesions are present in the considered datasets [7] and in general when the thinnest structures are of interest.

5. Conclusions

We have demonstrated the necessity of prior information during the iterative reconstruction of *ex vivo* cardiac datasets, to be performed in combination with the modelling of the scanner's resolution. The use of side anatomical information was not essential for our animal datasets, and a well-tuned

non-anatomical prior was sufficient for the recovery of the LV activity.

The analysis of the simulated data demonstrates that the Bowsher prior could have potential use in the recovery, delineation and analysis of the PET datasets, particularly if the thickness of the considered structures is expected to drop below the 4 mm.

6. New knowledge gained

This work addresses the previously unanswered question regarding the usefulness of anatomical and non-anatomical priors for the quantification of cardiac PET images. It provides guidelines for the reconstruction of cardiac emission datasets, partially confirming the results of previous literature on brain PVC, partially adding new insights into the usefulness of the prior information in the reconstruction of different cardiac structures. The study design using *ex vivo* cardiac datasets acquired on both a pre-clinical and a clinical scanner is innovative and original.

7. Competing interests

The authors declare that they have no competing interests.

8. Author's contributions

AT was responsible for the study design, the simulation setup, the reconstructions and the data collection and analysis, and drafted the manuscript. JN and KV assisted with the study design, the analysis of data and the careful revision of the manuscript. JUV, PC, JD and OG participated in the study design and critically revised the manuscript. All authors read and approved the final manuscript.

9. Acknowledgements

AT is a PhD fellow of the Research Foundation - Flanders (FWO). OG (1831812N) and JUV are senior clinical investigators of the Research Foundation - Flanders. KV is a post-doctoral researcher of the Research Foundation - Flanders.

The authors wish to thank Charles Watson, Judd Jones et al. for their help with the Siemens data processing, and Filip Rega for the development of the animal model used in this work.

[1] A. F. Schinkel, J. J. Bax, D. Poldermans, A. Elhendy, R. Ferrari, S. H. Rahimtoola, Hibernating myocardium: diagnosis and patient outcomes, Current problems in cardiology 32 (7) (2007) 375–410.

[2] J. Knuuti, H. R. Schelbert, J. J. Bax, The need for standardisation of cardiac FDG PET imaging in the evaluation of myocardial viability in patients with chronic ischaemic left ventricular dysfunction, European journal of nuclear medicine and molecular imaging 29 (9) (2002) 1257–1266.

[3] G. El Fakhri, A. Kardan, A. Sitek, S. Dorbala, N. Abi-Hatem, Y. Lahoud, A. Fischman, M. Coughlan, T. Yasuda, M. F. Di Carli, Reproducibility and accuracy of quantitative myocardial blood flow assessment with 82Rb PET: comparison with 13N-ammonia PET, Journal of Nuclear Medicine 50 (7) (2009) 1062–1071.

[4] M. Soret, S. L. Bacharach, I. Buvat, Partial-volume effect in PET tumor imaging, J. Nucl. Med. 48 (6) (2007) 932–945.

[5] A. M. Alessio, P. E. Kinahan, Improved quantitation for PET/CT image reconstruction with system modeling and anatomical priors., Med Phys 33 (2006) 4095:4103.

[6] K. Vunckx, A. Atre, K. Baete, A. Reilhac, C. M. Deroose, K. Van Laere, J. Nuyts, Evaluation of three MRI-based anatomical priors for quantitative PET brain imaging., IEEE Trans Med Imaging 31 (3) (2012) 599612.

[7] A. Turco, J. Nuyts, O. Gheysens, J. Duchenne, J.-U. Voigt, P. Claus, K. Vunckx, Lesion quantification and detection in myocardial 18F-FDG PET using edge-preserving priors and anatomical information from CT and MRI: a simulation study, EJNMMI physics 3 (1) (2016) 1–32.

[8] J. H. Hubbell, S. M. Seltzer, N. I. of Standards, T. (U.S.), Tables of X-ray mass attenuation coefficients and mass energy-absorption coefficients 1 keV to 20 MeV for elements Z=1 to 92 and 48 additional substances of dosimetric interest, U.S. Department of Commerce, Technology Administration, National Institute of Standards and Technology Gaithersburg, MD, web version. edn., URL

http://physics.nist.gov/PhysRefData/XrayMassCoef/cover.html, 1996.

[9] J. Bowsher, H. Yuan, L. Hedlund, T. Turkington, G. Akabani, A. Badea, W. Kurylo, C. Wheeler, G. Cofer, M. Dewhirst, G. Johnson, Utilizing MRI information to estimate F18-FDG distributions in rat flank tumors, in: Nuclear Science Symposium Conference Record, 2004 IEEE, vol. 4, 2488–2492 Vol. 4, 2004.

[10] K. Vunckx, J. Nuyts, Heuristic modification of an anatomical Markov prior improves its performance, in: Nuclear Science Symposium Conference Record (NSS/MIC), 2010 IEEE, 3262–3266, 2010.

[11] J. Nuyts, D. Beque, P. Dupont, L. Mortelmans, A concave prior penalizing relative differences for maximum-a-posteriori reconstruction in emission tomography, Nuclear Science, IEEE Transactions on 49 (1) (2002) 56–60.

[12] A. Chambolle, T. Pock, A First-Order Primal-Dual Algorithm for Convex Problems with Applications to Imaging, Journal of Mathematical Imaging and Vision 40 (1) (2011) 120–145.

[13] Y.-C. Tai, A. Ruangma, D. Rowland, S. Siegel, D. F. Newport, P. L. Chow, R. Laforest, Performance evaluation of the microPET focus: a third-generation microPET scanner dedicated to animal imaging, Journal of nuclear medicine 46 (3) (2005) 455–463.

[14] A. M. Alessio, A. Rahmim, Resolution modeling enhances PET imaging, Med. Phys 40 (2013) 120601.

[15] J. Nuyts, L. Mortelmans, P. Suetens, A. Oosterlinck, M. de Rou, Model-based quantification of myocardial perfusion images from SPECT, J. Nucl. Med. 30 (12) (1989) 1992–2001.

[16] M. D. Cerqueira, N. J. Weissman, V. Dilsizian, A. K. Jacobs, S. Kaul, W. K. Laskey, D. J. Pennell, J. A. Rumberger, T. Ryan, M. S. Verani, et al., Standardized myocardial segmentation and nomenclature for tomographic imaging of the heart a statement for healthcare professionals from the cardiac imaging committee of the Council on Clinical Cardiology of the American Heart Association, Circulation 105 (4) (2002) 539–542.

[17] K. Russell, M. Eriksen, L. Aaberge, N. Wilhelmsen, H. Skulstad, E. W. Remme, K. H. Haugaa, A. Opdahl, J. G. Fjeld, O. Gjesdal, T. Edvardsen, O. A. Smiseth, A novel clinical method for quantification of regional left ventricular pressure–strain loop area: a non-invasive index of myocardial work, European Heart Journal ISSN 0195-668X.

[18] J. Nuyts, Unconstrained image reconstruction with resolution modelling does not have a unique solution, EJNMMI physics 1 (1) (2014) 1.

[19] S. G. Nekolla, C. Rischpler, K. P. Kunze, PET/MRI for Cardiac Imaging: Technical Considerations and Potential Applications, in: Molecular and Multimodality Imaging in Cardiovascular Disease, Springer, 29–48, 2015.